Characterization of laser-produced fast electron sources for fast ignition

2010 Plasma Phys. Control. Fusion 52 124024

(http://iopscience.iop.org/0741-3335/52/12/124024)

Plasma Phys. Control. Fusion **52** (2010) 124024 (8pp) doi:10.1088/0741-3335/52/12/124024

Characterization of laser-produced fast electron sources for fast ignition

A Debayle[1], J J Honrubia[1], E d'Humières[2] and V T Tikhonchuk[2]

[1] ETSI Aeronáuticos, Universidad Politécnica de Madrid, Spain
[2] Université de Bordeaux-CNRS-CEA, CELIA, Talence, France

Received 5 July 2010, in final form 15 September 2010
Published 15 November 2010
Online at stacks.iop.org/PPCF/52/124024

Abstract
Laser-driven fast electron beams generated in planar foils or double cone targets have been characterized by means of two-dimensional particle-in-cell simulations. The laser beam focusing by the cone walls reduces the fast electron beam radius and increases the electron mean kinetic energy. Nevertheless, the beam divergence is high in both types of targets and can be split into two components: the dispersion angle and the radial velocity. The fast electron energy spectrum presents a power law profile. The effects of the fast electron source characteristics on the energy deposition in an 'ideal' precompressed inertial fusion target have been analysed. The radial velocity component of the fast electron beam significantly increases the energy required for ignition while the electron power law spectrum increases it slightly when compared with the standard exponential one.

(Some figures in this article are in colour only in the electronic version)

1. Introduction

High density currents of relativistic electrons can be produced by focusing an ultra-intense laser beam on a solid target. Based on this effect, an alternative inertial confinement fusion (ICF) scheme has been proposed. The electron-driven fast ignition scheme consists of separating the deuterium–tritium (DT) target compression by intense nanosecond laser beams from its heating by a laser-produced electron beam. The large distance between the relativistic electron source and the dense core found in typical ICF imploded targets can be reduced using a re-entrant cone inserted in the shell [1]. The cone also focuses the laser beam towards the cone tip inner surface [2] and generates electron wall currents [3] that reduce the fast electron (FE) beam divergence. The success of this scheme relies on a perfect knowledge of the FE beam characteristics dependence on the target and laser beam parameters. Due to the non-equilibrium heating of the plasma electrons in the laser standing wave and self-generated electric field [4], the fast electron spectrum can be far away from an exponential profile, as observed in kinetic simulations [5]. The FE divergence has been measured indirectly [6] and

far away from the source in the FE transport experiments carried out until now. It includes the FE divergence generated in the laser–plasma interaction region [7, 8], the resistive magnetic field collimation [9] and the Coulomb scattering. Experiments [10] have proven that the FE beam divergence increases with the laser intensity. This result is an evidence of the theory shown in [7], where the authors propose that the transverse electron momentum conservation in the laser evanescent wave is broken by the Weibel instability that develops in the laser–plasma interaction region. The stronger the Weibel instability induced magnetic fields, the stronger the electron scattering, leading to a high electron intrinsic dispersion angle. Also, the fast electron beam can gain a radial velocity [8]. The combined effect of both divergence components defines the initial evolution of the FE beam, which has a strong influence on the resistive magnetic field generation. It is worth noting that the initial beam radial velocity has been neglected so far in FE transport codes [11–13]. This approximation can lead to a strong over-estimation of the beam collimation by the resistive magnetic fields.

In this paper, we have extensively characterized the FE source produced by the interaction between an ultra-high intensity laser pulse and a planar foil with preplasma by means of two-dimensional (2D) planar particle-in-cell (PIC) simulations. The FE source characteristics are compared for planar foils and double cone targets, which may improve the FE source performance according to theoretical studies [3]. These results are presented in section 2. The effects of this more realistic electron source on the energy deposition in a compressed DT target using a 2D cylindrically symmetric hybrid code [14] are presented in section 3. The main results are briefly summarized in the conclusions.

2. Planar foil target versus double cone target

The PIC simulations are conducted with the code PICLS [15] in 2D planar geometry. The space and time resolutions were $\Delta x = \Delta z = c\Delta t = \lambda_0/56$ with $\lambda_0 = 1\,\mu$m the laser wavelength. Each cell contained 40 electrons and one gold ion. The ionization level is fixed to $Z = 40$ and the initial electron temperature is $T_e = 1$ keV for simulations without collisions and $T_e = 50$ eV for simulations with collisions. The simulation box size was $z \times x = 75 \times 50\,\mu\text{m}^2$ for the double cone target and $z \times x = 75 \times 70\,\mu\text{m}^2$ for the planar foil. Concerning this last case, the plasma has a maximum electron density of $n_e = 80 n_c$ where $n_c = 4\pi^2 m_e \varepsilon_0 c^2/e^2\lambda_0^2$ is the critical density. The plasma boundary was located at $z = 37.5\,\mu$m. As for a long preplasma, the fast electron energy deposition in the dense core decreases [16], we have assumed a small preplasma, exponentially decreasing with the scale length of $1\,\mu$m. The density map of the double cone is presented in figure 1(*a*). A preplasma with a scale length of $1\,\mu$m fills the cone interior. The laser beam propagates along the z-axis, from the left to the right and is p-polarized with the electric field in the x direction. The laser intensity has a Gaussian profile in the transverse direction and in time. The half-width-half-maximum (HWHM) radius is $10\,\mu$m, the HWHM pulse length is 210 fs and the maximum intensity $I_0 = 2 \times 10^{20}\,\text{W cm}^{-2}$. The FE source is characterized at the position $z = 42\,\mu$m, which is $\sim 1\,\mu$m behind the zone perturbed by the Weibel instability and the plasma hole boring. The FE distribution function was sampled in time and in the transverse direction for electron energies higher than 255 keV. The local FE divergence has been fitted by the formula: $f_l(\theta) = A \exp[-\ln 2(\theta - \theta_r)^2/\Delta\theta_0^2]$, where $\theta = \tan^{-1} p_x/p_z$, $\Delta\theta_0(x,t)$ is the local HWHM dispersion angle and $\theta_r(x,t)$ the local mean propagation angle. This latter accounts for the radial velocity of the FE beam.

We first discuss the collisionless simulations. A snapshot of the beam density is shown in figure 2(*a*) for both simulations with the planar foil (black line) and the double cone (red dotted line). The cone focuses the laser beam [2] towards the cone tip inner surface reducing thus the radius of the electron beam emission up to a value comparable to the inner cone outer

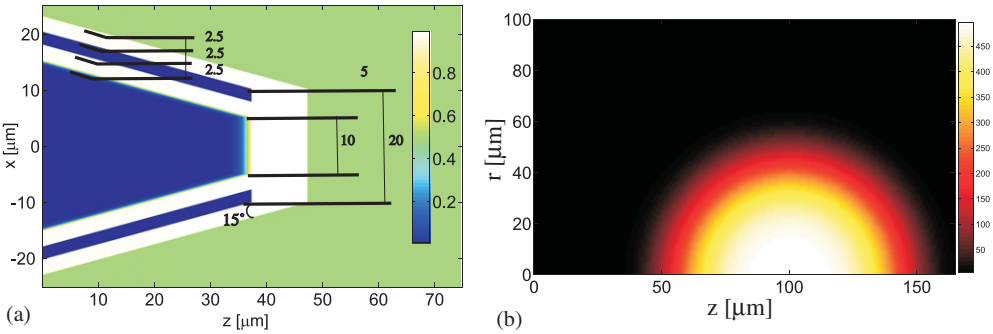

Figure 1. (*a*) Initial electron density map of the double cone, normalized to $80n_c$. (*b*) Density map in $\mathrm{g\,cm^{-3}}$ of the 'ideal' DT target considered for 2D cylindrically symmetric hybrid simulations. (Color online.)

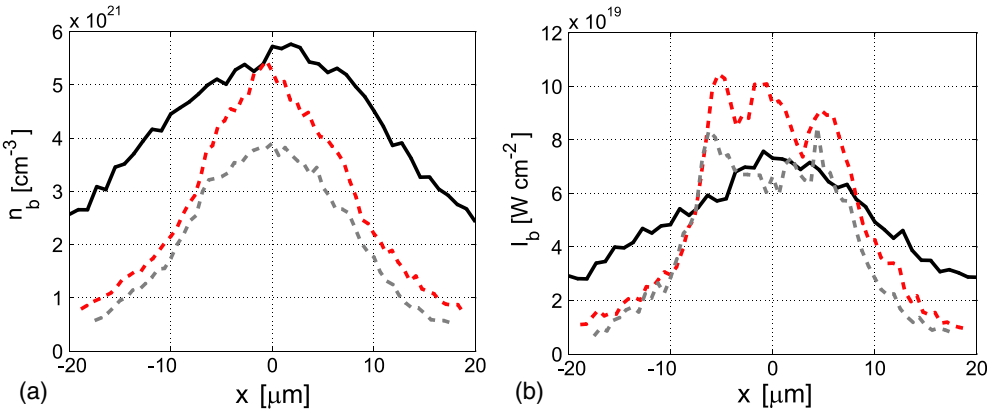

Figure 2. FE density (*a*) and surface energy flux (*b*) when the laser intensity in the cone tip reaches $I_0/2$. Legend is shown in figure 3(*b*). (Color online.)

radius, while it is two times higher ($r_b = 20\,\mu$m) than the laser focal spot ($r_0 = 10\,\mu$m) in the planar foil case. The beam density magnitude is comparable in both cases due to the superposition of the laser beam reflected from the cone walls and incident at 30° on the cone tip inner surface, with the normal incident laser beam. In this regime, the absorption occurs nearly at the same density than in the planar foil case. However, the mean electron energy is higher because the magnitude of the standing wave in front of the plasma is stronger. The FE spectrum integrated in the transverse direction is presented in figure 3(*a*) at the time when the laser intensity is $I = I_0/2$. In both cases, the FE spectrum presents a power law in the energy ranging from 100 keV to 10 MeV. In our collisionless simulation, when the laser intensity is around $I_0/2 = 10^{20}\,\mathrm{W\,cm^{-2}}$, the power law coefficient is 1.38 for the planar foil target, while it is 1.18 for the double cone. This apparently small difference implies a mean electron energy ∼40% higher in the double cone case. The corresponding mean electron energy is around 1.3 MeV in the double cone case, which is smaller than the ponderomotive scaling prediction consistent with experiments [17]. The surface energy flux at the same time as figure 2(*a*) is presented in figure 2(*b*). In the double cone geometry, the inner cone radius is two times smaller than the HWHM laser focal spot radius. Consequently, the energy flux is more intense than in the plane foil case but the integrated energy flux shown in figure 3(*b*) is comparable for

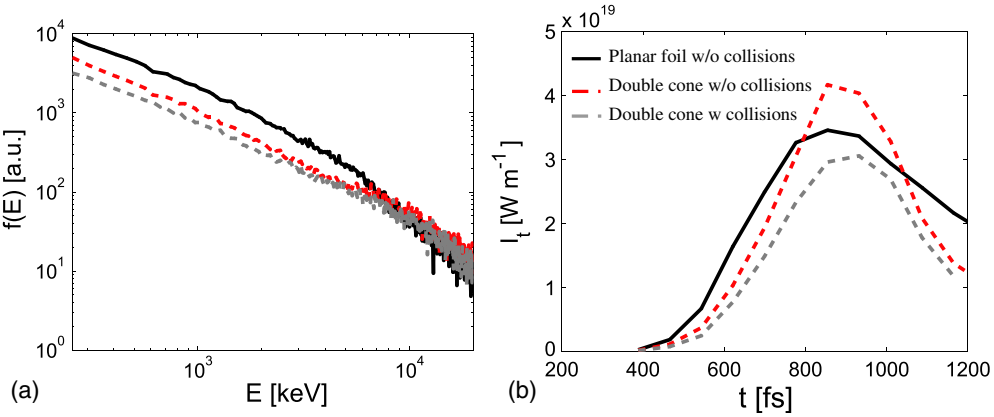

Figure 3. (*a*) Transverse integrated electron spectrum at the same time as figure 2. (*b*) Transverse integrated energy flux versus time. (Color online.)

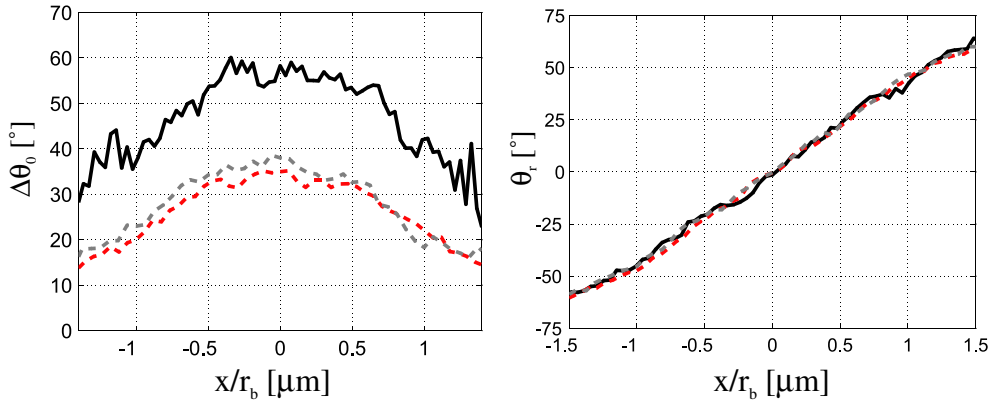

Figure 4. HWHM dispersion angle (*a*) and mean propagation angle (*b*) as a function of the transverse direction at the same time and with the same legend as figure 2. (Color online.)

both geometries. The transverse inhomogeneities of the energy flux, figure 2(*b*), are due to the laser interference at the cone tip [18]. Electrons gain more energy where the laser intensity is higher.

The local dispersion angle is presented in figure 4(*a*) at the same time as the snapshots of figure 2. In the case of the planar foil, the dispersion angle is larger. This is just a consequence of the beam ballistic propagation. In the planar foil case, the electron beam has a larger radius. Consequently, the beam requires a larger distance, $\sim r_\mathrm{b}/\Delta\theta_0$, before its dispersion will result in an increase in its radius [8]. As we characterize the FE source at the same depth in the plasma, the dispersion angle appears larger in the planar foil case. It is worth noting that the transverse velocity depending on the transverse direction, presented in figure 4(*b*), is high in both simulations. Indeed, due to the preplasma, the FE beam has a sufficient distance to convert its initial dispersion angle into radial velocity in the high density plasma. Without preplasma and for relatively short laser pulses, the laser–plasma interaction region is thin and the radial velocity is negligible [8]. In this case, the beam starts to propagate collimated and the resistive magnetic field generation is efficient to reduce the beam divergence even in the case of high

dispersion angle [19]. In our simulation cases, the local mean propagation angle θ_r cannot be neglected and represents, together with the dispersion angle, the relevant divergence parameters for our FE transport study. The effect of the radial velocity on the beam propagation has been neglected so far in FE transport codes used to reproduce experiments [20, 21] and to design the fast ignition scheme [14, 22]. Its effect is significant as it determines the length of beam ballistic propagation and, thus, the resistive magnetic field generation [8]. It is worthwhile pointing out that, in our simulation conditions, i.e. for a relatively long laser pulse with a high intensity and a high wall density, we do not observe any significant wall currents. The difference from the results presented in [2, 23, 24] may be due to the fact that a long and intense laser pulse expands the cone walls and breaks the condition of perfect solid interface required for the electron currents confinement near the walls. A high intensity laser pulse quickly generates a preplasma that decreases the confinement efficiency of the surface current by the magnetic field. Other publications have already reported on the absence of significant wall currents [18, 25] and a parametric study of the surface current generation is required in order to increase the cone efficiency [26].

In collisionless simulations, the Weibel instability induced magnetic fields may be overestimated. In order to check the effect of collisions, we ran the simulation of laser impinging on a double cone with an electron density of $80n_c$, while the collision rate was calculated assuming solid gold. Since the fast electron acceleration occurs in the preplasma, where collisions are weak, we found that the collisions do not have any significant effect on the beam divergence. This can be seen in figures 4(*a*) and (*b*) where we present the local dispersion angle and the radial velocity, respectively. There is a very small difference between the collisionless simulation (red dotted line) and the simulation with collisions (grey dotted line). The collisional effect on the beam density, the FE spectrum and the surface and linear energy fluxes are shown in figures 2 and 3. The collisions reduce slightly the absorption by ∼20% compared with the collisionless simulations.

3. Effects of FE source characteristics on fast ignition energy threshold

We have studied the effects of the FE source characteristics on energy deposition into a simple dense core for fast ignition with a 2D cylindrically symmetric hybrid code [14]. The density map of the DT core is represented in figure 1(*b*). The super-Gaussian density distribution has a peak value of 500 g cm^{-3} with a HWHM radius of 45 μm and its center is located 100 μm far from the left surface from which fast electrons are injected. The minimum density is 1.4 g cm^{-3}. The initial plasma temperature is $T_e = T_i = 300$ eV. The FE source divergence is generalized to 2D cylindrical geometry according to the following formula:

$$f_l = \exp\left[-\ln 2\left(\frac{\tan^{-1}[\sqrt{(p_r\cos\theta_r - p_z\sin\theta_r)^2 + p_\varphi^2}/|p_z\cos\theta_r + p_r\sin\theta_r|]}{\Delta\theta_0}\right)^2\right], \quad (1)$$

where $\theta_r = \theta_0 r/r_b$, r is the radial position, p_r is the radial electron momentum, p_φ is the azimuthal electron momentum and p_z is the longitudinal electron momentum. The standard beam divergence assumed in FE transport codes [20, 21] corresponds to $\theta_0 = 0$. The beam electron spectrum $f(\gamma)$ can be represented either by an exponential function $f(\gamma) \propto \exp[-m_e c^2\gamma/T]$ or by a power law function $f(\gamma) \propto ((\gamma_0 - 1)/(\gamma - 1))^a$, where γ is the electron Lorentz factor, and a and γ_0 are parameters to be fitted to PIC simulations. Other beam parameters are a HWHM radius $r_b = 20\,\mu$m with a transverse Gaussian profile, and a HWHM beam length of 10 ps with a Gaussian profile in time.

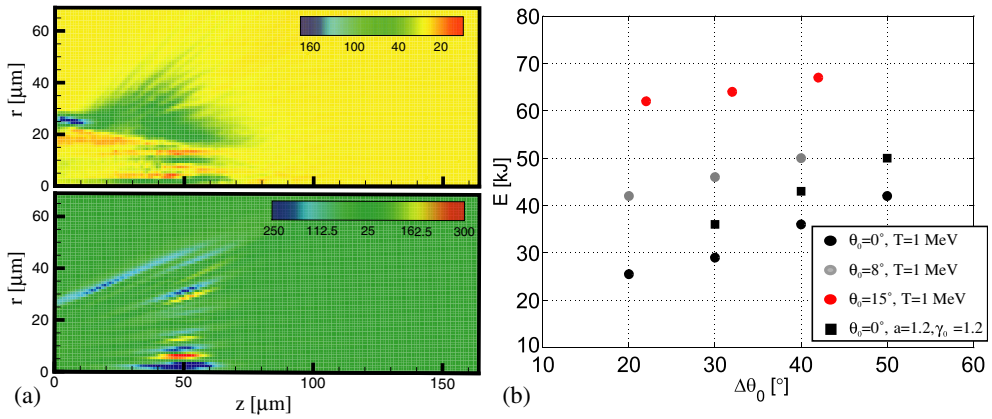

Figure 5. (*a*) Azimuthal magnetic field in T at $t = 1$ ps, for the beam divergence parameters $\Delta\theta_0 = 40^\circ$ and $\theta_0 = 0^\circ$ (top panel), and for $\Delta\theta_0 = 22^\circ$ and $\theta_0 = 15^\circ$ (bottom panel). (*b*) Electron beam energy required for the DT ignition as a function of the HWHM dispersion angle for different beam parameters. (Color online.)

We first discuss the effect of the electron beam radial velocity θ_r. In the top panel of figure 5(*a*), we present a snapshot of the magnetic field at the beginning of simulation $t = 1$ ps for the beam divergence parameters, $\Delta\theta_0 = 40^\circ$ and $\theta_0 = 0^\circ$. The FE spectrum is exponential with a mean energy $T = 1$ MeV. The main magnetic field surrounding the beam is generated according to the Faraday law, $\partial_t \boldsymbol{B} = -\nabla \wedge \boldsymbol{E}$. Initially, and near the laser–plasma interaction region, the magnetic field is thus generated such as $\partial_t B_\theta \approx \eta \partial_r j_{bz}$, with j_{bz} the longitudinal beam current density and η the plasma resistivity. The magnetic field maximum is located near the maximum gradient in the radial direction of the longitudinal current around the beam radius $r(z)$. In the simulation shown in figure 5(*a*), top panel, the radial velocity is zero, and the beam starts its propagation parallel to the axis. The beam divergence becomes visible at a certain distance where the electrons, which have started to propagate from the beam center with the characteristic angle $\theta = \Delta\theta_0$, cross the trajectory of electrons that have started to propagate parallel to the axis at the position r_b. This occurs at the depth $z \sim r_\mathrm{b}/\Delta\theta_0 \sim 20\ \mu$m. The beam radius evolution is not a linear function of z but an hyperbolic function of z, as observed in other simulations [21]. In figure 5(*a*), bottom panel, we present the same simulation but with the dispersion angle $\Delta\theta_0 = 22^\circ$ and the radial velocity at HWHM $\theta_0 = 15^\circ$, which gives the same HWHM divergence angle of the full angular distribution function $f(\theta) = \int r\mathrm{d}r f_l(\theta) \cos\theta$ than the previous case $\Delta\theta_0 = 40^\circ$. Clearly, the resistive magnetic field penetration depth is reduced as the beam radius starts to increase linearly with the initial mean propagation angle θ_0. In the rigid beam approximation [8], the length reduction factor is of the order of $1 - \theta_0/\Delta\theta_0$. Figure 5(*b*) shows the dependence of the beam energy required for ignition on the dispersion angle and the radial velocity. The presence of radial velocity increases significantly the electron beam energy required for ignition. While without radial velocity a beam with dispersion angle $\Delta\theta_0 = 50^\circ$ ignites the fuel with an energy of 43 kJ, a beam with a radial velocity of 15° and a HWHM dispersion angle of 32° ignites only with an energy of 65 kJ. Such a study is not quantitative in the sense that the beam parameters are not related to the laser beam characteristics. However, it gives an estimate of the beam energy required for DT ignition, as previous studies, which did not take into account the beam radial velocity, are probably too optimistic [12, 22]. If the beam radial velocity is taken into account, the ignition energies would rise at least by a factor of ∼2 for θ_0 as low as 15°.

We have also estimated the influence of the electron spectrum on the energy deposition in the core. According to the FE source study presented in the previous section, the FE beam has a power law spectrum with a coefficient $a \sim 1.2$ for electron energies between 100 keV and 7 MeV. Compared with the exponential profile with the equivalent temperature of $T \sim 1$ MeV, the low energy electrons carry ∼10–20% more energy in the case of a power law spectrum. Correspondingly, as it is shown in figure 5(*b*), 10–20% more beam energy is required to ignite the compressed fuel. Although this effect is less significant compared with that of radial velocity, it corresponds to a laser beam energy increases by an additional factor of 10–20%.

4. Conclusions

We have studied the characteristics of the fast electron source produced by the interaction between an ultra-high intensity laser beam, $I > 10^{20}$ W cm^{-2}, with a planar foil and a double cone target. In both cases, the fast electron divergence is high and it is composed of two components: angular dispersion and transverse velocity. The angular dispersion is due to the electron scattering in the small scale magnetic fields that appear in the laser–plasma interaction region due to Weibel instability [7]. It is higher in the case of preplasma as the background electron density is smaller. The radial divergence is mainly due to the beam electron opening in the laser–plasma interaction region extended over several micrometers due to the preplasma [8]. The fast electron spectrum is different from the standard exponential profile for low energy electrons as it presents a power law structure [5]. As already observed in experiments [27], the main effect of the cone consists of focusing the laser beam towards the cone tip inner surface [2], thus increasing the mean electron kinetic energy and reducing the electron beam radius. No wall currents were observed in our simulation conditions, i.e. for a high laser intensity and a long pulse, consistent with experiments [25]. The power law structure of the electron spectrum and the radial velocity have been neglected so far in fast electron transport codes used for the fast ignition scheme studies. The power law spectrum has a relatively small effect on the energy deposition into the dense core that can be explained by an increased number of low energy electrons compared with an exponential spectrum. The radial electron velocity decreases substantially the resistive magnetic field generation, and thus the beam collimation and the energy deposition in the dense core, rising the ignition threshold by a factor of ∼2 or higher.

Acknowledgments

This work has been partially supported by the HiPER project and the research grant ENE2009-11668 from the Spanish Ministry of Education and Research. Calculations have been performed at the CESVIMA, CINES and CCRT supercomputing centers.

References

[1] Kodama R *et al* 2001 *Nature* **412** 798
[2] Sentoku Y *et al* 2004 *Phys. Plasmas* **11** 3083
[3] Cai H-B *et al* 2009 *Phys. Rev. Lett.* **102** 245001
[4] Wilks S C *et al* 1992 *Phys. Rev. Lett.* **69** 1383
[5] Ren C *et al* 2004 *Phys. Rev. Lett.* **93** 185004
[6] Lancaster K L *et al* 2007 *Phys. Rev. Lett.* **98** 125002
[7] Adam J C, Héron A and Laval G 2006 *Phys. Rev. Lett.* **97** 205006
[8] Debayle A *et al* 2010 *Phys. Rev.* E **82** 036405
[9] Bell A R and Kingham R J 2003 *Phys. Rev. Lett.* **91** 035003

[10] Green J S *et al* 2008 *Phys. Rev. Lett.* **100** 015003
[11] Welch D R *et al* 2006 *Phys. Plasmas* **13** 063105
[12] Honrubia J J and Meyer-ter-Vehn J 2006 *Nucl. Fusion* **46** L25 (arXiv:physics/0605249)
[13] Johzaki T, Nakao Y and Mima K 2009 *Phys. Plasmas* **16** 062706
[14] Honrubia J J and Meyer-ter-Vehn J 2009 *Plasma Phys. Control. Fusion* **51** 014008
[15] Sentoku Y and Kemp A J 2008 *J. Comput. Phys.* **227** 6846
[16] MacPhee A G *et al* 2010 *Phys. Rev. Lett.* **104** 055002
[17] Tanimoto T *et al* 2009 *Phys. Plasmas* **16** 062703
[18] Baton S D etal 2008 *Phys. Plasmas* **15** 042706
[19] Storm M *et al* 2009 *Phys. Rev. Lett.* **102** 235004
[20] Gremillet L, Bonnaud G and Amiranoff F 2002 *Phys. Plasmas* **9** 941
[21] Honrubia J J, Antonicci A and Moreno D 2004 *Laser Part. Beams* **22** 129
[22] Johzaki T *et al* 2009 *Plasma Phys. Control. Fusion* **51** 014002
[23] Habara H *et al* 2006 *Phys. Rev. Lett.* **97** 095004
[24] Psikal J *et al* 2010 *Phys. Plasmas* **17** 013102
[25] van Woerkom L *et al* 2008 *Phys. Plasmas* **15** 056304
[26] Micheau S *et al* 2010 *Phys. Plasmas* at press
[27] Chen Z L *et al* 2005 *Phys. Rev.* E **71** 036403